Journal of Sound and Vibration (2001) **239**(5), 931–948
doi:10.1006/jsvi.2000.3193, available online at http://www.idealibrary.com on IDEAL®

ESTIMATION OF SEA COUPLING LOSS FACTORS USING A DUAL FORMULATION AND FEM MODAL INFORMATION, PART II: NUMERICAL APPLICATIONS

L. MAXIT AND J.-L. GUYADER

INSA de Lyon (*National Institute of Applied Sciences*), *L.V.A.* (*Vibrations-Acoustic Laboratory*), *Bat*. 303, 20, *avenue Albert Einstein*, 69621 *Villeurbanne Cedex*, *France*
E-mail: *maxit@lva.insa-lyon.fr*, *guyader@lva.insa-lyon.fr*

(*Received* 28 *June* 1999, *and in final form* 25 *January* 2000)

Numerical applications of the approach presented in a companion paper is proposed for the cases of coupled beams and coupled plates. Results are compared with other calculations. CLF calculations for coupled beams are achieved with an analytical modal description. The influences of thickness ratio and damping on the quality of the prediction are presented and discussed. CLF determination with an FEM modal description are then applied to the case of two thin plates coupled in an L shape. This case allows comparison with other calculations and will be a representative of the applicability of the method to more complex structures such as industrial ones. The good agreement with other methods validates the calculation of CLF with the present method.

1. INTRODUCTION

In an earlier companion paper [1], a theoretical method was presented to calculate the coupling loss factor from modal information of subsystem. By using dual modal formulation and an appropriate subsystem mode definition, the expression which has to be obtained (see (68) of reference [1]) allows CLF to be determined only from a knowledge of the modes of the uncoupled-subsystems and damping information. In the case of complex subsystems, the modal information can be calculated by finite element method. The mode shapes are then described by nodal variables (displacements or forces) and the interaction modal work between a couple of modes can be evaluated by considering the discretized mode (see [1], section 4).

In this paper, numerical applications of the approach are proposed to illustrate the method and to validate it against other methods. Before going on to perform CLF calculations with FEM, an example of coupled beams is used to determine CLF from the dual modal formulation. In this section, modes are calculated analytically and results are compared with "exact" calculations for different thickness ratios and different damping loss factors of the beams.

Validation of the CLF calculation with FEM data are then presented. An example of L-shaped plates is considered, which is representative of the applicability of the method to more complex structures and allows the method to be compared with the results given by the SEA inverse matrix technique with numerical experiments.

0022-460X/01/050931 + 18 $35.00/0

2. A FIRST EXAMPLE

2.1. PRESENTATION

This example is based on two Euler–Bernoulli beams coupled rigidly at one end as shown in Figure 1. The beams of rectangular section are simply supported at their ends, and the coupling is expressed by continuity conditions on the flexural moments and the angular rotations.

$L_\alpha, b_\alpha, h_\alpha, E_\alpha, \rho_\alpha, \nu_\alpha$ are, respectively, length, width, thickness, Young's modulus, mass density, and Poisson's coefficient of beam α. Then the cross-sectional area is $S_\alpha = b_\alpha h_\alpha$ and the surface inertia of beam α is $I_\alpha = 12^{-1} b_\alpha (h_\alpha)^3$. In co-ordinate x_i $(i = 1, 2, 3)$, the variables W_i^1 and W_i^2 $(i = 1, 2, 3)$ represent the displacements and σ_{ij}^1 and σ_{ij}^2 are the stress tensors associated to beams 1 and 2 respectively. A local co-ordinate system (x, y, z) is represented in Figure 1. (A list of nomenclature is given in B.)

The Euler–Bernoulli assumptions on displacements and stresses for beam α are

$$W_1^\alpha(x, y, z, t) = -y \frac{\partial W_y^\alpha}{\partial x}(x, t), \quad W_2^\alpha(x, y, z, t) = W_y^\alpha(x, t), \quad W_3^\alpha(x, y, z, t) = 0, \quad \alpha = 1, 2 \tag{1}$$

where $W_y^\alpha(x, t)$ is the generalized transversal displacement of beam α. Also

$$\sigma_{11}^\alpha(x, y, z, t) = y\sigma_x^\alpha(x, t), \quad \sigma_{ij}^\alpha(x, y, z, t) = 0, \quad \alpha = 1, 2 \tag{2}$$

where $\sigma_x^\alpha(x, t)$ is the generalized normal stress of beam α.

2.2. ANALYTICAL DESCRIPTION

The beams are supposed to be made of the same material (aluminium) but it makes the hypothesis that beam 1 is thinner than beam 2. The consequence is that beam 1 will vibrate as if it is clamped at its coupling end and beam 2 will vibrate as if it is simply supported at its coupling end. The subsystem definitions are then deduced naturally to be the uncoupled-blocked subsystem for beam 1 and the uncoupled-free subsystem for beam 2. The boundary conditions for the extraction of subsystem modes are simply supported-clamped for beam 1, and simply supported–simply supported for beam 2 (see Figure 2).

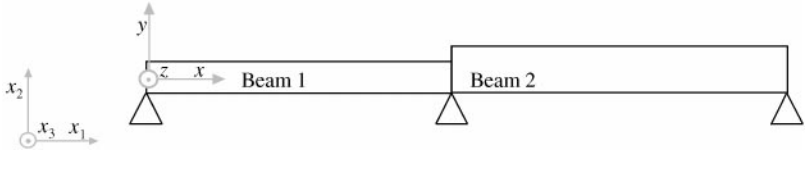

Figure 1. Two pinned–pinned beams coupled rigidly at one end.

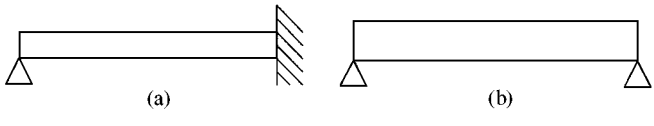

Figure 2. Uncoupled beams: (a) uncoupled-blocked subsystem, beam 1; (b) uncoupled-free subsystem, beam 2.

Then subsystem 1 could have a stress description, and subsystem 2 could have a displacement description. It is not necessary to re-develop the dual modal formulation, because it is very simple to use the results of section 3 directly and the physical interpretation of the interaction modal work to determinate the modal coupling coefficients, γ_{pq}^{12}. In this example, the dual variables are the flexural moment and the angular rotation. The flexural moment, $\mathbf{M}_p^1$, is associated with beam 1 (stress description) and the angular rotation, θ_z^2, is associated with beam 2 (displacement description). The interaction modal work exchanged by the pth mode of beam 1 and the qth mode of beam 2, $\mathbf{W}_{pq}^{12}$, is expressed by the product of the flexural moment of the pth mode and the angular rotation of the qth mode at the coupling end,

$$\mathbf{W}_{pq}^{12} = \tilde{\mathbf{M}}_f^{1p}(L_1)\tilde{\theta}_z^{2q}(L_1), \tag{3}$$

where $\tilde{\mathbf{M}}_f^{1p}(L_1)$ is the flexural moment of mode p of beam 1 at the coupling end, and $\tilde{\theta}_z^{2q}(L_1)$ is the angular rotation of mode q of beam 2 at the coupling end.

Euler–Bernouilli theory gives

$$\tilde{\mathbf{M}}_f^{1p}(x) = I_1\tilde{\sigma}_x^{1p}(x), \quad \text{where } \tilde{\sigma}_x^{1p}(x) \text{ is the stress shape of mode } p \text{ of beam 1,} \tag{4}$$

$$\tilde{\theta}_z^{2q}(x) = \frac{\partial \tilde{W}_y^{2q}}{\partial x}(x), \quad \text{where } \tilde{W}_y^{2q}(x) \text{ is the displacement shape of mode } q \text{ of beam 2.} \tag{5}$$

To evaluate CLF from equation (68) of Part 1, modes for each beam must be calculated. The information necessary for beam 1 includes natural frequencies, generalized mass and stress mode shapes at the coupling end, and for beam 2, includes frequencies, generalized mass and displacement mode shapes at the coupling end.

For beam 1, modal analysis is developed in Appendix A where two methods are presented to evaluate the stress mode shapes. Finally, the modal information can be expressed by (for $\omega_p^1 \neq 0$)

$$\omega_p^1 = \sqrt{\frac{E_1 I_1}{\rho_1 S_1}}\,(k_p^1)^2 \quad \text{with } k_p^1/\tan(k_p^1 L_1) = \tanh(k_p^1 L_1), \tag{6}$$

$$M_p^1 = \rho_1 S_1 L_1, \tag{7}$$

$$\tilde{\sigma}_x^{1p}(x) = (k_p^1)^2 E_1 I_1 \Bigg[\cosh(k_p^1(L_1 - x)) + \cos(k_p^1(L_1 - x)) - \frac{\cosh(k_p^1 L_1) - \cos(k_p^1 L_1)}{\sinh(k_p^1 L_1) - \sin(k_p^1 L_1)} (\sinh(k_p^1(L_1 - x)) + \sin(k_p^1(L_1 - x))) \Bigg], \tag{8}$$

where ω_p^1 is the natural angular frequency and M_p^1 the generalized mass of mode p.

For beam 2, the subsystem modal information is classical:

$$\omega_q^2 = \sqrt{\frac{E_2 I_2}{\rho_2 S_2}}\,(k_q^2)^2 \quad \text{with } k_q^2 = \frac{q\pi}{L_2}, \tag{9}$$

$$M_q^2 = \frac{\rho_2 S_2 L_2}{2}, \tag{10}$$

$$\tilde{W}_y^{2q}(x) = \sin(k_q^2(x - L_2)), \tag{11}$$

where ω_q^2 is the natural angular frequency and M_q^2 the generalized mass of mode q.

From equations (4,5,8,11), the expression for the interaction modal work (3) is

$$\mathbf{W}_{pq}^{12} = 2(k_p^1)^2 E_1 I_1 k_q^2. \tag{12}$$

Note that the modal information necessary to evaluate the interaction modal work is only the mode shape at the coupling end.

The CLF must be evaluated by taking into account only the coupling between the resonant modes in the frequency bandwidth $\Delta\omega$ considered, these resonant modes being chosen to represent to physical modes of the global structure, it justifies that they describe the global behaviour of the structure in the frequency bandwidth. One note N_1^1 and N_2^1 (resp. N_1^2 and N_2^2), the modal orders of resonant modes with the lowest and highest natural frequencies in $\Delta\omega$ for beam 1 (and beam 2). The number of resonant modes is $N_1 = N_2^1 - N_1^1 + 1$ for beam 1 and $N_2 = N_2^2 - N_1^2 + 1$ for beam 2.

Then, with equation (68) of part 1, equations (6, 7), (10–12), the CLF is expressed by

$$\eta_{12} = \frac{1}{N_1 \omega_1} \sum_{p=N_1^1}^{N_2^1} \sum_{q=N_1^2}^{N_2^2} \left\{ \frac{8(k_q^2)^2 E_1 I_1}{L_1 L_2 \rho_2 S_2} \left[\frac{[\Delta_p^1 (\omega_q^2)^2 + \Delta_q^2 (\omega_p^1)^2]}{((\omega_p^1)^2 - (\omega_q^2)^2)^2 + (\Delta_p^1 + \Delta_q^2)(\Delta_p^1 (\omega_q^2)^2 + \Delta_q^2 (\omega_p^1)^2)} \right] \right\}, \tag{13}$$

where Δ_p^1, Δ_q^2 are the modal damping bandwidths.

It can be noticed that the damping loss factor can be attributed independently to each mode of each subsystem. However, in classical SEA, one global damping loss factor affects each subsystem for all the modes of the frequency bandwidth. It is assumed that

$$\Delta_p^1 = \omega_p^1 \eta_1, \quad \forall p \in [N_1^1 N_2^1], \quad \Delta_q^2 = \omega_q^2 \eta_2, \quad \forall q \in [N_1^2, N_2^2], \tag{14}$$

where η_1 and η_2 are the DLFs of beam 1 (and beam 2), respectively.

With this assumption, (13) becomes

$$\eta_{12} = \frac{1}{N_1 \omega_t} \sum_{p=N_1^1}^{N_2^1} \sum_{q=N_1^2}^{N_2^2} \times \left\{ \frac{8(k_q^2)^2 E_1 I_1}{L_1 L_2 \rho_2 S_2} \left[\frac{[\eta_1 \omega_p^1 (\omega_q^2)^2 + \eta_2 \omega_q^2 (\omega_p^1)^2]}{((\omega_p^1)^2 - (\omega_q^2)^2)^2 + (\eta_1 \omega_p^1 + \eta_2 \omega_q^2)(\eta_1 \omega_p^1 (\omega_q^2)^2 + \eta_2 \omega_q^2 (\omega_p^1)^2)} \right] \right\}. \tag{15}$$

2.3. NUMERICAL RESULTS

The present approach is compared to the results yielded by the SEA matrix-inversion technique with numerical experiment (see reference [2]). Euler–Bernoulli theory and wave decomposition is used to simulate the numerical experiment. The "rain on the roof" excitation on beam 1 is approximated by averaging beam energy over 20 randomly distributed points of excitation. The potential and kinetic energy obtained by the wave decomposition for a given angular frequency are spatial and frequency averaged. The coupling loss factor, η_{12}^{ne}, is finally evaluated by introducing beam energies into the SEA relation when subsystem 2 is not excited,

$$\eta_{12}^{ne} = \frac{\eta_2 \langle E_t^2 \rangle}{\langle E_t^1 \rangle - (n_1/n_2) \langle E_t^2 \rangle}, \tag{16}$$

where $\langle E_t^{\alpha} \rangle$ is the total energy of beam α obtained from numerical experiment, and n_α is the asymptotic modal density of beam α given by the analytical expression

$$n_\alpha = L_\alpha \omega_c^{1/2} \left(\frac{\rho_\alpha S_\alpha}{E_\alpha I_\alpha} \right)^{1/4}, \tag{17}$$

in which ω_c is the central angular radian frequency of the frequency bandwidth.

The results given by equation (15) are called the "CLF dual modal formulation" or, in short, CLF DMF, and the results given by the numerical experiment and equation (16) is called "SEA matrix-inversion".

In the following, the values $E_\alpha = 7 \times 10^{+10}$ N/m^2, $v_\alpha = 0.3$, $\rho_\alpha = 2700$ kg/m^3, $\alpha = 1, 2$ are always used.

2.3.1. *Intermodal coupling factors*

The intermodal coupling factors, β_{pq}^{12} are shown in Figure 3 as a function of couples of resonant modes of the two beams. (Note that the CLF are obtained by summing up all these factors (see equation (15)):

$$\beta_{pq}^{12} = \left[\frac{8(k_q^2)^2 E_1 I_1}{L_1 L_2 \rho_2 S_2} \right] \left[\frac{[\eta_1 \omega_p^1 (\omega_q^2)^2 + \eta_2 \omega_q^2 (\omega_p^1)^2]}{((\omega_p^1)^2 - (\omega_q^2)^2)^2 + (\eta_1 \omega_p^1 + \eta_2 \omega_q^2)(\eta_1 \omega_p^1 (\omega_q^2)^2 + \eta_2 \omega_q^2 (\omega_p^1)^2)} \right]. \tag{18}$$

Generally speaking, the intermodal coupling factors vary considerably with the mode couple. This is due to two phenomena: the spatial coincidence of mode shapes at the connections; the frequency coincidence (second bracket in equation (18)).

In case of point connection, the frequency coincidence effect dominates and the intermodal coupling factor is strong when $\omega_p^1 \approx \omega_q^2$ (see Figure 3).

2.3.2. *Results for different thickness ratio of the two beams*

Figure 4 shows the CLF versus third-octave band for four different beam thickness ratios. There is a good agreement between the results from the approach developed in this paper

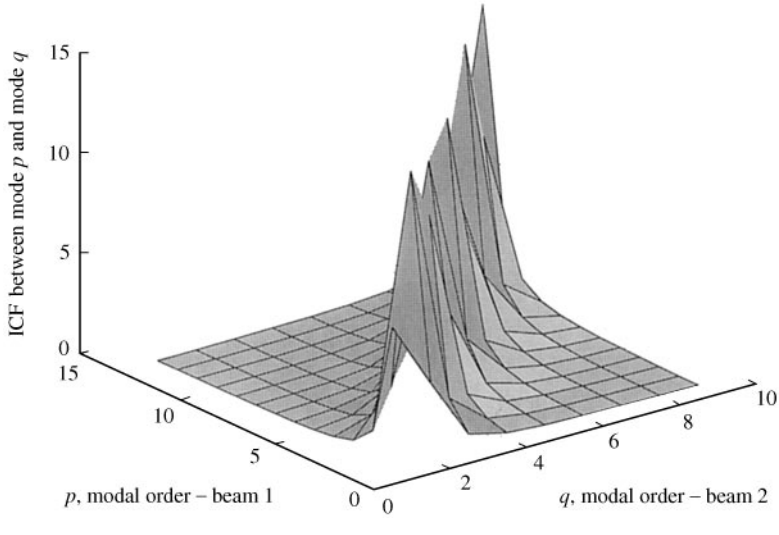

Figure 3. Intermodal coupling factors versus couples of resonant modes of the two beams, third-octave band 16 000 Hz; $L_1 = 2{\cdot}5$ m, $L_2 = 3{\cdot}5$ m, $b_1 = b_2 = 0{\cdot}01$ m, $h_1 = 0{\cdot}001$ m, $h_2 = 0{\cdot}004$ m, $\eta_1 = \eta_2 = 0{\cdot}01$.

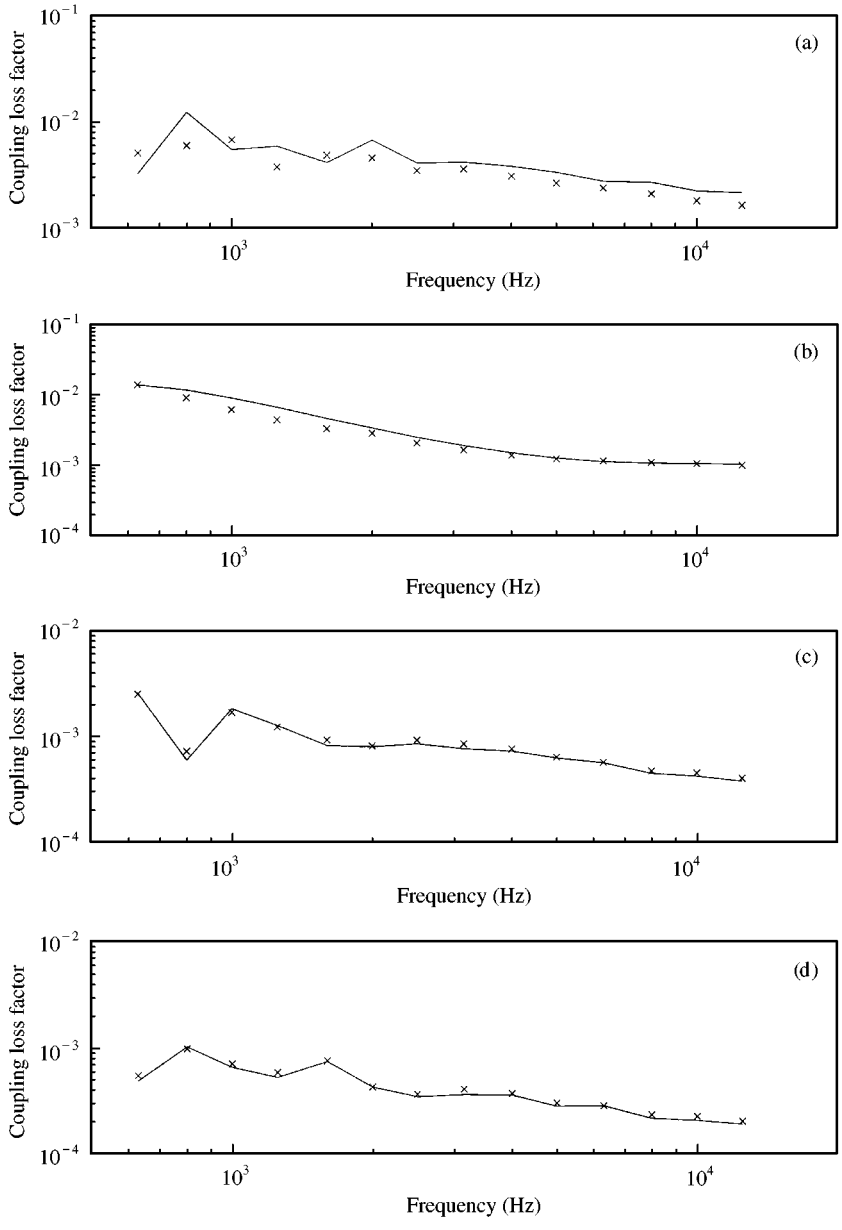

Figure 4. Coupling loss factor versus frequency; one-third-octave band results; (a) $h_2/h_1 = 1{\cdot}5$, (b) $h_2/h_1 = 2$, (c) $h_2/h_1 = 3$, (d) $h_2/h_1 = 4$; $L_1 = 2{\cdot}5$ m, $L_2 = 3{\cdot}5$ m, $b_1 = b_2 = 0{\cdot}01$ m, $h_1 = 0{\cdot}001$ m, $\eta_1 = \eta_2 = 0{\cdot}01$. Two calculations: ——, present approach; ×, SEA matrix-inversion.

and the results from numerical experiment. This is true even when the thickness ratio is near unity but a small difference (see Figure 4(a)) is observed due to an increase of coupling strength. In this case, the difference in impedance between the two subsystems is not sufficient to ensure that the resonant modes in the frequency band are able to represent completely the vibratory behaviour of the coupled subsystems.

An extreme case is shown in Figure 5 where the coupling of two identical beams is considered. In this situation, the choice of subsystem modes is arbitrary but in accordance

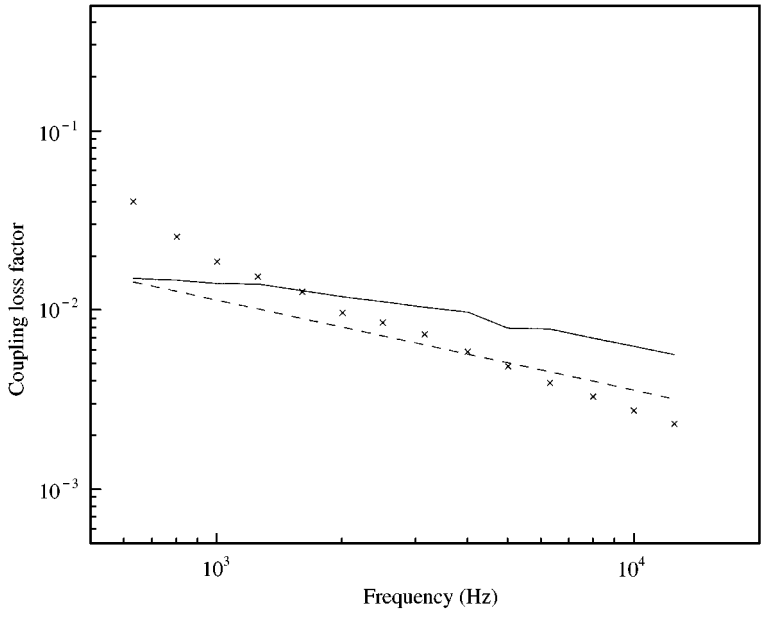

Figure 5. Coupling loss factor versus frequency; one third-octave-band results; $L_1 = L_2 - 2{\cdot}5$ m, $b_1 = b_2 = 0{\cdot}01$ m, $h_1 = h_2 = 0{\cdot}001$ m, $\eta_1 = \eta_2 = 0{\cdot}01$. Three calculations: ——, present approach; ×, SEA matrix-inversion; - - - -, travelling wave approach.

with the dual modal formulation, one subsystem should be blocked and the other should be free. The results given by the traditional wave approach (see expression (96) in reference [3]) are also plotted. As was foreseeable, some differences are noted between the results given by the two approaches and the "exact" results. These differences are not so important (less than 5 dB), and show that even in a severe coupling case, the results given by the present approach are not unsatisfactory. The improved wave theory given in reference [3], which does not require the many assumptions necessary for SEA, can be more suitable for this system of beams of equal thickness.

2.3.3. *Comparison results given by two opposite choices of modes*

Figure 6 shows the coupling loss factor versus the thickness ratio h_1/h_2. Two calculations by the present approach have been made: the first, which is plotted as a solid line, considers blocked modes for beam 1 and free modes for beam 2, whereas, the second, which is plotted as a dashed line, considers free modes for beam 1 and blocked modes for beam 2. The modes are then reversed between the two calculations.

When the thickness ratio is less than one, the subsystem modes used by the first calculation suited well, whereas the second calculation gives poor results. Inversely, when the thickness ratio is greater than one, the subsystem modes used by the second calculation are the most appropriate.

It must be emphasized that the choice of subsystem modes used to calculate the CLF by the present approach is not arbitrary. It should be chosen so that the subsystem modes are closest to the physical modes of the global structure. For example, when $h_1/h_2 < l$, beam 1 is thinner than beam 2 and will it vibrate rather as if it is clamped at its coupling end whereas beam 2 will vibrate rather like a beam simply supported at its coupling end. In this case, it can be deduced that beam 1 should be represented by the modes of the

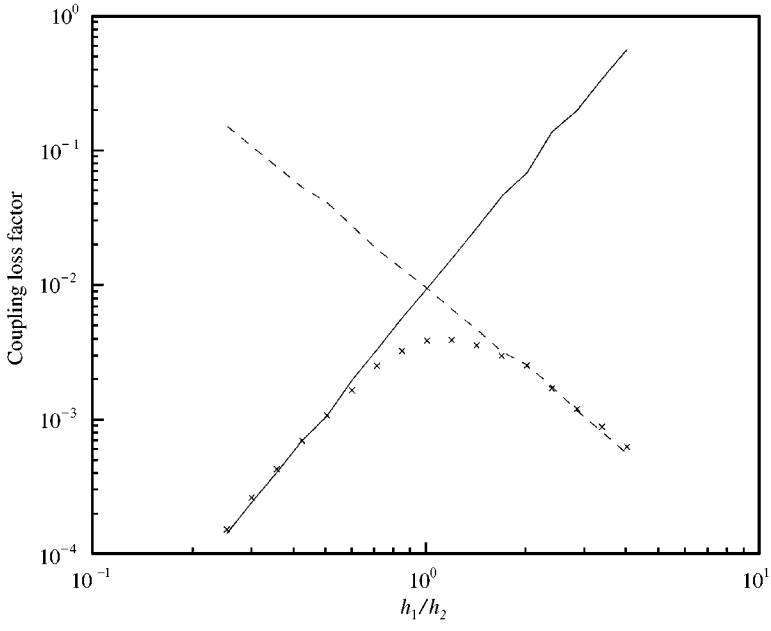

Figure 6. Coupling loss factor versus thickness ratio h_1/h_2; third-octave band centred on 10 000 Hz; $L_1 = 2{\cdot}5$ m, $L_2 = 3{\cdot}5$ m, $b_1 = b_2 = 0{\cdot}01$ m, $h_1 = 0{\cdot}001$ m, $\eta_1 = \eta_2 = 0{\cdot}01$. Three calculations: ——, present approach with blocked modes for beam 1 and free modes for beam 2; - - - -, present approach with free modes for beam 1 and blocked modes for beam 2; ×, SEA matrix-inversion.

uncoupled-blocked subsystem, whereas beam 2 should be represented by the modes of the uncoupled-free subsystem.

As in the previous section, some slight errors are noted for beams of equal thickness whatever the choice of modes (which become arbitrary in this case).

2.3.4. *Results for different damping*

Figure 7 shows the coupling loss factor versus third-octave band when the damping loss factor of the beam is modified. In Figure 7(a–c) the DLF are the same for the two beams. Good agreement can be seen between both methods of calculation. In the case of low damping, the difference is larger (see Figure 7(c)). In such a situation, a more detailed approach (SmEdA) presented in references [4, 5] can be used which allows better results to be obtained. This method allows modal energy distribution to be taken into account and the calculations from the intermodal coupling factors accurate energy results when modal overlap is low.

In Figure 7(d), the case of different damping loss factors for the two beams is investigated. As previously, the presented method agrees well with the classical calculation in equation (16).

It can be noticed from the results given here that the CLF values depend slightly on damping which justifies the classical travelling wave approach which gives results that are independent of damping. However, for very low damping, the damping dependence of CLF is more important (see references [3, 6]) and in this case, SmEdA approach can be necessary (see references [4, 5]).

The present approach agrees with the numerical experiment method but has major advantages of giving CLF without solving equations, but only by making an analogy with basic SEA modelization. The computation time is thus very short.

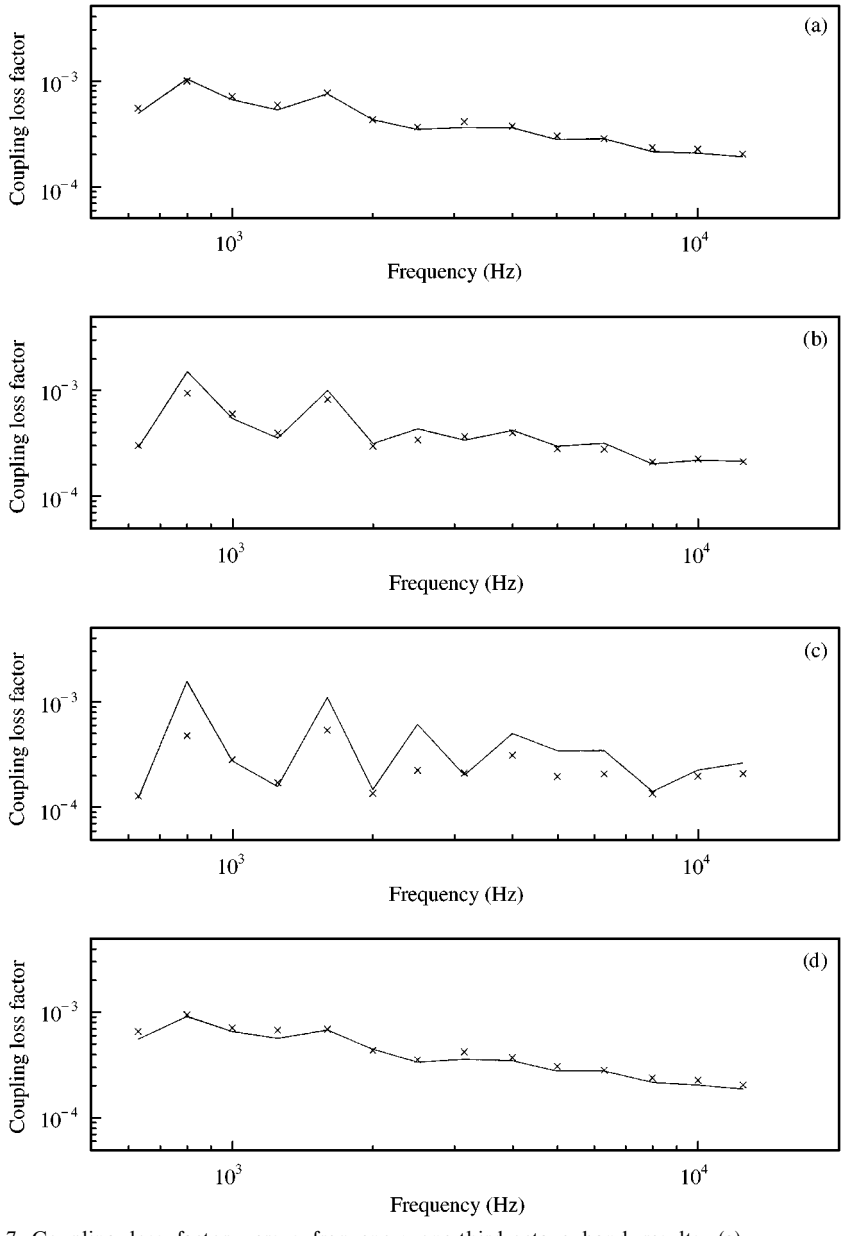

Figure 7. Coupling loss factor versus frequency; one-third-octave band results. (a) $\eta_1 = \eta_2 = 0{\cdot}01$; (b) $\eta_1 = \eta_2 = 0{\cdot}005$; (c) $\eta_1 = \eta_2 = 0{\cdot}002$; (d) $\eta_1 = 0{\cdot}02$, $\eta_2 = 0{\cdot}005$, $L_1 = 2{\cdot}5$ m, $L_2 = 3{\cdot}5$ m, $b_1 = b_2 = 0{\cdot}01$ m, $h_1 = 0{\cdot}001$ m, $h_2 = 0{\cdot}004$ m. Two calculations: ——, present approach; ×, SEA matrix-inversion.

3. APPLICATION OF CLF DETERMINATION WITH FEM DATA

To demonstrate the validity of the approach, the simple case of two-coupled homogeneous plates in an L shape, shown in Figure 8, is considered.

From the finite element point of view, the matrix form of the equation of motion is the same for both complicated and simple structures. So, in principle, the problem treated will be representative of the applicability of the method to more complicated cases. In addition, this case allows a comparison with another calculation to be made.

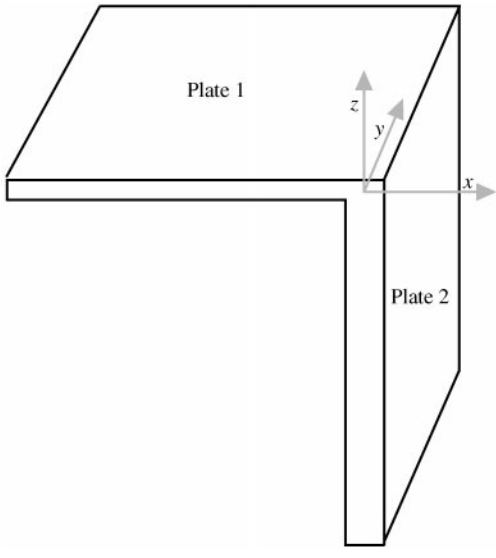

Figure 8. Illustration of an **L**-shaped plate.

TABLE 1

Definition and values of parameters

	Plate 1	Plate 2
Length of the common edge	$A_1 = 1$ m	$A_2 = 1$ m
Other length	$B_1 = 1$ m	$B_2 = 2{\cdot}5$ m
Thickness	$H_1 = 3$ mm	$H_2 = 12$ mm
Modulus of elasticity	$E_1 = 2\times10^{+11}$ Pa	$E_2 = 2\times10^{+11}$ Pa
Density	$\rho_1 = 7800$ kg/M^3	$\rho_2 = 7800$ kg/M^3
Poisson's ratio	$\nu_1 = 0{\cdot}3$	$\nu_2 = 0{\cdot}3$
Damping loss factor	$\eta_1 = 0{\cdot}02$	$\eta_2 = 0{\cdot}02$

Thin plate theory is assumed and only bending motion is considered. All the non-coupled edges of each plate are supposed to be simply supported. The parameter definitions and their values are presented in Table 1.

Plate 1 is thinner than plate 2, so that it must be described by modes of the uncoupled-blocked subsystem, and plate 2 must be described by modes of the uncoupled-free subsystem. Thus, for subsystem definitions, plate 1 is clamped on the coupling edge and simply supported on the others edges. Plate 2 is simply supported along all the edges.

3.1. FINITE ELEMENT MODEL

The finite element model of each subsystem is generated and analysed by UAI/NASTRAN v11.8 package and by using the QUAD4 Element. The numbers of nodes of the regular meshes are chosen in order to have a minimum of 10 elements at natural wavelength at 3000 Hz. Then, for plate 1 there are 100 nodes along each edges, and for

TABLE 2

Definition of the extracted FEM output data for each plate. i: node on the common edge (coupling node set); generalized masses normalized to one

	Mode order	Natural frequency	Mode shape on common edge $i \in \{\text{Coupling node set}\}$
Plate 1	p	$\omega_p^1/$ $1\text{ Hz} < \dfrac{\omega_p^1}{2\pi} < 3000\text{ Hz}$	"SINGLE POINT CONSTRAINT FORCE" SPCFORCE $\rightarrow \{\tilde{f}_{p1}^{1i}, \tilde{f}_{p2}^{1i}, \tilde{f}_{p3}^{1i}, \tilde{f}_{p4}^{1i}, \tilde{f}_{p5}^{1i}, \tilde{f}_{p6}^{1i}\}$
Plate 2	q	$\omega_q^2/$ $1\text{ Hz} < \dfrac{\omega_q^2}{2\pi} < 3000\text{ Hz}$	"DISPLACEMENT" DISPLACEMENT $\rightarrow \{\tilde{u}_{q1}^{2i}, \tilde{u}_{q2}^{2i}, \tilde{u}_{q3}^{2i}, \tilde{u}_{q4}^{2i}, \tilde{u}_{q5}^{2i}, \tilde{u}_{q6}^{2i}\}$

plate 2 there are 100 nodes for the smallest edge in order to have coincidence meshing and 130 nodes for the other one. Appropriate boundary conditions and Lanczos method are used to calculate the modes between 1 and 3000 Hz for each plate. The generalized masses are normalized to one. The NASTRAN output data for each mode are the natural frequency, the "SINGLE POINT CONSTRAINT FORCE" for plate 1, and the "DISPLACEMENT" for plate 2. As the present approach requires only the mode shapes on the coupling boundary, it is possible to select only the nodes on the coupling boundary as an output set (coupling node set). That allows the size of the NASTRAN output files to be limited. For example, for plate 1, this output set is composed of the nodes, which are fixed, and the shape output data are described by the "SINGLE POINT CONSTRAINT FORCE". The output necessary for the CLF determination (see Table 2) are extracted from the NASTRAN output files and are analysed by a MATLAB program.

Equation (80) of Part I [1] is used to determine the interaction modal work from nodal components of mode shapes. In the case of flexural plates coupling, only the 5th force nodal component for plate 1 (y-component of bending moment) and the 5th displacement nodal component for plate 2 (y-component of angular rotation) are not null for the nodes of the coupling node set. Then, the interaction modal work between mode p of plate 1 and mode q of plate 2 can be reduced to

$$W_{pq}^{12} = \sum_{i \in \{\substack{Coupling \\ node\ \ set}\}} \tilde{f}_{p5}^{1i}\, \tilde{u}_{q5}^{2i}, \tag{19}$$

where $\tilde{f}_{p5}^{1i}$ is the 5th nodal component force of node i representing the y-component bending moment of the pth mode of plate 1, and $\tilde{u}_{q5}^{2i}$ is the 5th nodal component displacement of node i representing the y-component angular rotation of the qth mode of plate 2.

3.2. MODAL DENSITY COMPARISON

To check the validity of the FEM models in the frequency band of interest, it is possible to count the natural frequencies (see Table 3), and then to determine the modal density for each frequency band and finally to compare it with the asymptotic value n_α given by

$$n_\alpha = \frac{\sqrt{3} A_\alpha B_\alpha}{H_\alpha \sqrt{E_\alpha/\rho_\alpha (1 - \nu_\alpha)}}, \quad \alpha = 1, 2 \text{ (modes/Hz)}. \tag{20}$$

TABLE 3
Number of modes per band for each plate; finite element results

	315 Hz	400 Hz	500 Hz	630 Hz	800 Hz	1000 Hz	1250 Hz	1600 Hz	2000 Hz	2500 Hz
Plate 1	7	9	13	12	19	25	27	38	47	57
Plate 2	5	4	8	8	12	15	17	22	32	40

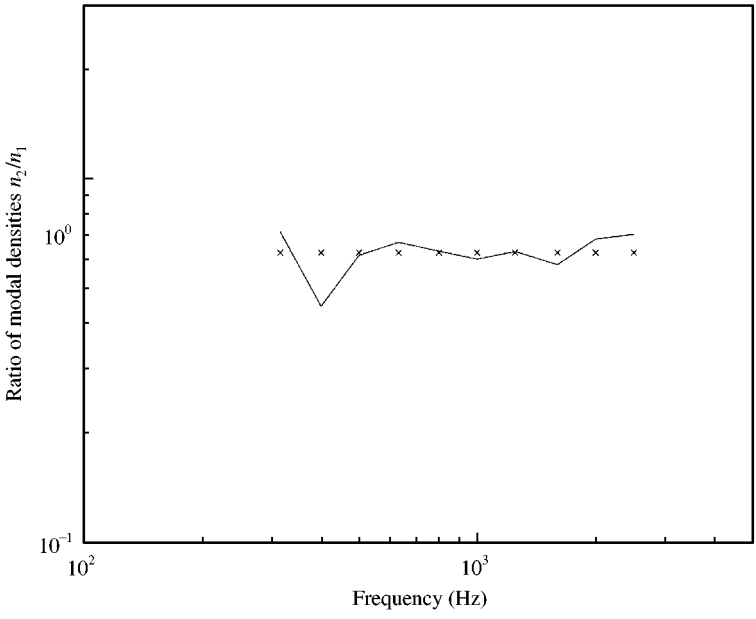

Figure 9. Modal densities ratio versus frequency, third-octave band calculation. ——, FEM result; × with expression (20).

This is presented in Figure 9 where the modal density ratio between the two subsystems is plotted versus third octave band. It can be concluded that the FEM modelization represents of the vibration behaviour of the plates well in the frequency range of interest. It is well known that the eigenfrequencies and the mode shapes of the finite element model may be shifted to the real eigenfrequencies and mode shapes at "high frequency" even in the case of a correct element model. However, as explained in reference [7], these numerical errors seem to be reduced by averaging the data.

3.3. COUPLING LOSS FACTOR COMPARISON

From the expression of the interaction modal work for a discretized system (19) and with the FEM data described in section 3.1, on the coupling loss factor (with (68) of part I) can be evaluated, this result is called the CLF-DMF/FEM.

In the same manner as that in section 2, the present approach with FEM data is compared to the results yielded by the SEA matrix-inversion technique with numerical experiment. The "exact" results of the numerical experiment are obtained from the dual modal formulation with an analytical modal description. A comparison with the general

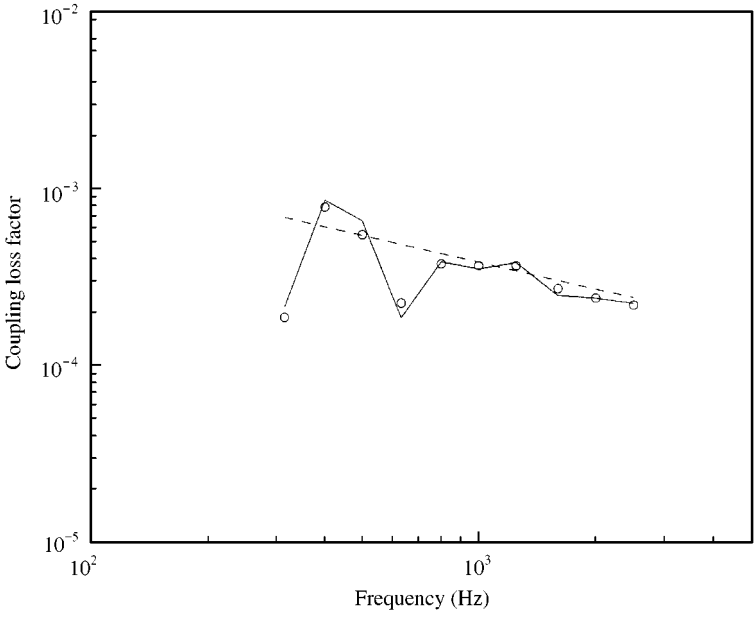

Figure 10. Coupling loss factor versus frequency, third-octave band calculation. Three calculations: ——, CLF-DMF/FEM; ○, SEA matrix-inversion; - - - -, travelling wave approach.

dynamic stiffness method allows the convergence of the model series to be checked. The "rain on the roof" excitation on plate 2 is approximated by averaging plate energy over 15 points of excitation randomly distributed. Energies are spatial and frequency averaged. CLF is finally calculated by introducing plate energies into the SEA relation when subsystem 1 is not excited,

$$\eta_{12}^{ne} = \frac{\eta_1 \langle E_t^1 \rangle}{n_1/n_2 \langle E_t^2 \rangle - \langle E_t^1 \rangle}, \tag{21}$$

where $\langle E_t^\alpha \rangle$ is the total energy of plate α obtained from numerical experiment, and n_α is the modal density of plate α given by equation (20).

Figure 10 shows a comparison of three techniques of CLF calculation; the two techniques previously described and the classical technique derived from the travelling wave approach (see equations (20–23) in reference [8]).

There is a good agreement between the three results in high frequency. Below 800 Hz, the travelling wave approach which considers semi-infinite plates gives poor results for some third-octave bands whereas the present approach takes the coupling between the two plates into account correctly.

Figure 11 shows an SEA calculation using the CLF-DMF/FEM when plate 2 is excited. This calculation is compared to an exact calculation (used previously in the SEA matrix-inversion technique). Good agreement can be seen which clearly validates the calculation of CLF with the present method.

The important variations of energy ratios for the frequency bands below 1000 Hz can be explained by the fact that there are few resonant modes which participate to the coupling in these bands. Indeed, Figure 12 shows the intermodal coupling factors for the third-octave band centred on 800 Hz. Although plate 1 has 20 resonant modes in the frequency band and plate 2 has 12 resonant modes, only two couples of modes contribute significantly to the

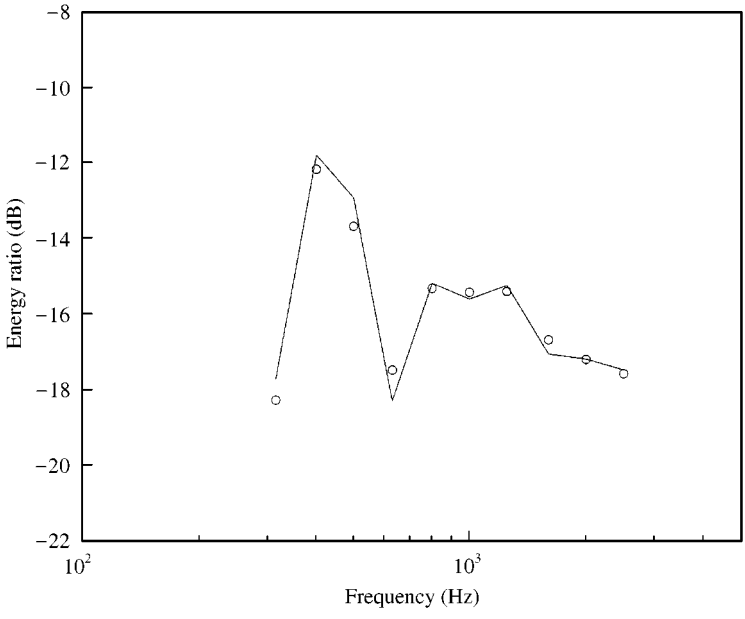

Figure 11. Energy ratio E1/E2 versus frequency, third-octave band calculation, plate 2 excited. Two calculations: ——, SEA result with CLF obtained by DMF/FEM; ○, exact result.

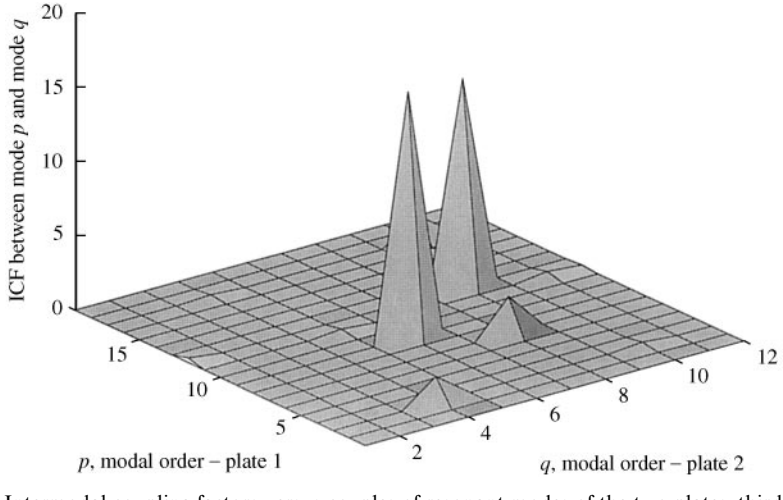

Figure 12. Intermodal coupling factors versus couples of resonant modes of the two plates, third-octave band 800 Hz; DMF/FEM results; modes classified with increasing natural frequencies.

coupling of the plates. Contrary to beam coupling, the spatial coincidence has an important effect which leads some couples of modes to be uncoupled.

As for beams of equal section (see section 2.3.2), the coupling of plates of equal thickness is a limit to the application of the present approach. Some slight errors will be made by this approach because the resonant subsystem modes which are considered could not fully represent the behaviour of the coupled plates. In this case of two edges-coupled rectangular plates of equal thickness, the calculations proposed by Wester and Mace [9] can be more appropriate because they do not require the numerous SEA assumptions.

4. CONCLUSIONS

Beam examples have verified the validity of the CLF determination with the dual modal formulation and basic SEA relation for power flow in oscillators having gyroscopic coupling. It is shown that results are good when SEA assumptions are followed.

On the other hand, it has been seen that the present approach can be used in connection with FEM. Application of the SEA-CLF/FEM technique gives good estimates of vibrational energy ratios between two coupled plates for the third-octave band between 315 and 2500 Hz. Although eigenfrequency shifts occur in FEM calculations at high frequency, good results are obtained for CLF. This is due to the averaging over several couples of modes participating to the transfer. The simple plate example has been chosen to allow comparison. The application to more complicated structures is straightforward because the technique is based on any general finite element model. It can be noticed that heterogeneous substructures having three-dimensional vibration motions can be treated without difficulty by the CLF-DMF/FEM technique.

When a subsystem has a low number of modes in the frequency band, SEA can give a poor estimate of energy transfer, because some assumptions used in the method are not realistic (in particular equipartition). The approach described in the two companion papers is a starting point for an extension of SEA to non-modal energy equipartition in subsystems. This SEA extension called statistical modal energy distribution analysis (SmEdA) is briefly presented in reference [4] and will be developed in another paper. The purpose of SmEdA is to extend the validity of SEA to systems of low modal density.

ACKNOWLEDGMENTS

The authors are grateful for the interest and financial support of DGA/DSP-CNRS (Direction des Systèmes de forces et de la Prospective) and CTSN Toulon (Centre Technique des Systèmes Navals), without which this work would not have been done.

REFERENCES

1. Part I paper.
2. C. SIMMONS and C. FREDO 1990 *Internoise*'90. *International Conference on Noise Control Engineering, Gothenburg, Sweden.* Vibration analysis of coupled stiffened plates using the finite element method.
3. B. R. MACE 1993 *Journal of Sound and Vibration* **166**, 429–461. The statistical energy analysis of two continuous one-dimensional subsystems.
4. L. MAXIT and J. L. GUYADER 1999 *Sixth International Congress on Sound and Vibration, Copenhagen, Denmark*, 5–8 *July*. Statistical modal energy distribution analysis (SmEdA).
5. L. MAXIT 2000 *Ph.D. Thesis, Institut National des Sciences Appliquées de Lyon, France*. Extension et reformulation de modèle SEA par la prise en compte de la répartition des énergies modales.
6. F. F. YAP and J. WOODHOUSE 1996 *Journal of Sound and Vibration* **197**, 351–371. Investigation of damping effects on statistical energy analysis of coupled structures.
7. C. SIMMONS 1991 *Journal of Sound and Vibration* **144**, 215–227. Structure-borne sound transmission through plate junctions and estimates of SEA coupling loss factors using finite element method.
8. D. A. BIES and S. HAMID 1980 *Journal of Sound and Vibration* **70**, 187–204. In situ determination of coupling loss factors by the power injection method.
9. E. C. N. WESTER and B. R. MACE 1996 *Journal of Sound and Vibration* **193**, 793–822. Statistical energy analysis of two edge-coupled rectangular plates: ensemble averages.
10. O. BERNASCONI and D. J. EWINS 1989 *Journal of Modal Analysis* **4**, 68–76. Modal strain/stress fields.

APPENDIX A: MODAL ANALYSIS OF UNCOUPLED-BLOCKED BEAM 1

Without applied forces and displacement, the free motion of the uncoupled-blocked subsystem (beam 1) can be represented by the following equations:

$$\rho_1 S_1 \frac{\partial^2 W_y^1}{\partial t^2}(x,t) + I_1 \frac{\partial^2 \sigma_x^1}{\partial x^2}(x,t) = 0 \quad \forall x \in]0, L_1[, \tag{A1}$$

$$-E_1 I_1 \frac{\partial^2 W_y^1}{\partial x^2}(x,t) + I_1 \sigma_x^1(x,t) = 0 \quad \forall x \in]0, L_1[, \tag{A2}$$

$$W_y^1(0,t) = 0, \quad I_1 \sigma_x^1(0,t) = 0, \tag{A3}$$

$$W_y^1(L_1,t) = 0, \quad \frac{\partial \tilde{W}_y^1}{\partial x}(L_1,t) = 0. \tag{A4}$$

Two methods can be used to obtain the natural frequencies and the stress mode shapes:

First method, by analogy between the stress eigenvalue problem, and the equivalent displacement eigenvalue problem.

To obtain the stress problem, the time second derivation of equation (A2) should be combined with equation (A1):

$$\rho_1 S_1 \frac{\partial \sigma_x^1}{\partial t^2}(x,t) + E_1 I_1 \frac{\partial^4 \sigma_x^1}{\partial x^4}(x,t) = 0 \quad \forall x \in]0, L_1[, \tag{A5}$$

$$I_1 \frac{\partial^2 \sigma_x^1}{\partial x^2}(0,t) = 0, \quad I_1 \sigma_x^1(0,t) = 0, \quad I_1 \frac{\partial^2 \sigma_x^1}{\partial x^2}(L_1,t) = 0, \quad I_1 \frac{\partial^3 \sigma_x^1}{\partial x^3}(L_1,t) = 0. \tag{A6}$$

After a separation of time and space,

$$\sigma_x^{1p}(x,t) = \tilde{\sigma}_x^{1p}(x) \mathrm{e}^{(\mathrm{j}\omega_p^1 t)}, \tag{A7}$$

the stress eigenvalue problem can be written

$$-\rho_1 S_1 (\omega_p^1) \tilde{\sigma}_x^{1p}(x) + E_1 I_1 \frac{\partial^4 \tilde{\sigma}_x^{1p}}{\partial x^4}(x) = 0 \quad \forall x \in]0, L_1[, \tag{A8}$$

$$I_1 \frac{\partial^2 \tilde{\sigma}_x^{1p}}{\partial x^2}(0) = 0, \quad I_1 \tilde{\sigma}_x^{1p}(0) = 0, \quad I_1 \frac{\partial^2 \tilde{\sigma}_x^{1p}}{\partial x^2}(L_1) = 0, \quad I_1 \frac{\partial^3 \tilde{\sigma}_x^{1p}}{\partial x^3}(L_1) = 0. \tag{A9}$$

This problem is analogous to classical displacement eigenvalue problem of a beam simply supported in $x = 0$ and free in $x = L_1$. Then, the solutions can be expressed by ($\omega_p^1 \neq 0$)

$$\omega_p^1 = \sqrt{\frac{E_1 I_1}{\rho_1 S_1}} (k_p^1)^2 \quad \text{with } k_p^1 / \tan(k_p^1 L_1) = \tanh(k_p^1 L_1),$$

$$\int_0^{L_1} \rho_1 S_1 (\tilde{\sigma}_x^{1p}(x))^2 \, \mathrm{d}x = \rho_1 S_1 L_1, \tag{A10}$$

$$\tilde{\sigma}_x^{1p}(x) = \cosh(k_p^1(L_1 - x)) + \cos(k_p^1(L_1 - x))$$

$$- \frac{\cosh(k_p^1 L_1) - \cos(k_p^1 L_1)}{\sinh(k_p^1 L_1) - \sin(k_p^1 L_1)} \cdot (\sinh(k_p^1(L_1 - x)) + \sin(k_p^1(L_1 - x))).$$

As the Helmholtz mode for an acoustic cavity problem, the simply supported-clamped beam has one stress mode of null natural frequency (see section 3.4.2 of Part I). Indeed by analogy with displacement equation of motion, this mode corresponds to the rigid body mode of the simply supported-free beam. It is expressed by

$$\omega_0^1 = 0, \qquad \tilde{\sigma}_x^{1,0}(x) = x. \tag{A11}$$

This method of calculation of stress mode shapes can be used only for simple structures where the analogy with displacement equations is possible. This method does not permit the generalized mass or the generalized stiffness as defined in section 3 of Part I [1] (equations (45)–(49)) to be obtained directly.

Second method, by the calculation of the displacement mode shapes of the displacement eigenvalue problem and by using the constitutive law (see reference [10]).

The displacement eigenvalue problem is obtained directly by introducing equation (A1) in equation (A2) and by taking into account boundary conditions.

With a separation of time and space $W_y^1(x,t) = \tilde{W}^{1p}(x)\,e^{j\omega_p^1 t}$, solutions of the problem are finally

$$\omega_p^1 = \sqrt{\frac{E_1 I_1}{\rho_1 S_1}}(k_p^1)^2 \quad \text{with } k_p^1/\tan(k_p^1 L_1) = \tanh(k_p^1 L_1),$$

$$M_p^1 = \rho_1 S_1 L_1,$$

$$\tilde{W}_y^{1p}(x) = \cosh(k_p^1(L_1 - x)) - \cos(k_p^1(L_1 - x))$$

$$- \frac{\cosh(k_p^1 L_1) - \cos(k_p^1 L_1)}{\sinh(k_p^1 L_1) - \sin(k_p^1 L_1)} \cdot (\sinh(k_p^1(L_1 - x)) - \sin(k_p^1(L_1 - x))). \tag{A12}$$

Using the constitutive law (A2), gives the stress shape associated to the pth mode is

$$\tilde{\sigma}_x^{1p}(x) = (k_p^1)^2 E_1 I_1 \Bigg[\cosh(k_p^1(L_1 - x)) + \cos(k_p^1(L_1 - x))$$

$$- \frac{\cosh(k_p^1 L_1) - \cos(k_p^1 L_1)}{\sinh(k_p^1 L_1) - \sin(k_p^1 L_1)} \cdot (\sinh(k_p^1(L_1 - x)) + \sin(k_p^1(L_1 - x))) \Bigg]. \tag{A13}$$

By this calculation the stress mode of null frequency cannot be determined. However, this is not important for the CLF determination because this mode is always non-resonant and thus it is not necessary to take it into account.

APPENDIX B: NOMENCLATURE

A_1, A_2	plate length of the common edge
b_1, b_2	beam width
B_1, B_2	plate length
E_1, E_2	Young's modulus
$\langle E_t^1 \rangle, \langle E_t^2 \rangle$	averaged total energy obtained from numerical experiment

f_k^{1t}, f_k^{2t} force nodal variable
$\tilde{f}_{pk}^{1t}, \tilde{f}_{qk}^{2t}$ force nodal mode shape
h_1, h_2 beam thickness
H_1, H_2 plate thickness
I_1, I_2 beam second moment area
k_p^1, k_p^2 modal wave number
K_p^1, K_q^2 modal stiffness
L_1, L_2 beam length
$\tilde{\mathbf{M}}_f^{1p}$ flexural moment mode shape of beam 1
M_p^1, M_q^2 modal mass
n_1, n_2 modal density
N_1, N_2 number of resonant modes in the considered frequency bandwidth
N_1^1, N_1^2 modal order of resonant mode with the lowest natural frequency in $\Delta\omega$
N_2^1, N_2^2 modal order of resonant mode with the highest natural frequency in $\Delta\omega$
S_1, S_2 beam cross-section
u_k^{1i}, u_k^{2i} displacement nodal variable
$\tilde{u}_{pk}^{1i}, \tilde{u}_{qk}^{2i}$ displacement nodal mode shape
$\mathbf{W}_{pq}^{12}$ interaction modal work between mode p of subsystem 1 and mode q of subsystem 2
W_t^n, W_t^n displacement vector
W_y^1, W_y^2 beam generalized transversal displacement
$\tilde{W}_y^{1p}, \tilde{W}_y^{2q}$ generalized displacement mode shape
β_{pq}^{12} intermodal coupling factor (ICF) between mode p of subsystem 1 and mode q of subsystem 2
$\Delta\omega$ angular frequency bandwidth of interest
Δ_p^1, Δ_q^2 modal damping bandwidth
η_{12} coupling loss factor (CLF)
η_{12}^{ne} CLF obtained by SEA matrix-inversion technique with numerical experiment
η_1, η_2 damping loss factor (DLF)
γ_{pq}^{12} gyroscopic modal coupling coefficient between mode p of subsystem 1 and mode q of subsystem 2
ν_1, ν_2 Poisson's coefficient
$\tilde{\theta}_t^{2q}$ angular rotation mode shape of beam 2
ω_c central angular radian frequency of the frequency bandwidth $\Delta\omega$
ω_p^1, ω_q^2 mode's natural angular frequency
ρ_1, ρ_2 mass density
$\sigma_{ij}^1, \sigma_{ij}^2$ stress tensor
σ_x^1, σ_x^2 beam generalized normal stress
$\tilde{\sigma}_x^{1p}$ generalized stress mode shape of beam 1